Characterization of a high voltage nanosecond-pulsed atmospheric pressure He plasma jet and its treatment on deionized water and different cell media

M. J. Seong, Y. J. Ha, H. S. Kwon, S. J. Kim, H. M. Joh and T. H. Chung

Department of Physics, Dong-A University, Busan, Korea

Abstract: In this work, a high voltage nanosecond-pulsed APPJ is fabricated and utilized to treat the deionized water and different cell media. Characterization of nanosecond-pulsed plasma and its unique features and merits for biomedical applications are explored in comparison with those of low frequency or microsecond-pulsed APPJ. Compared to microsecond-pulse APPJ, the nanosecond-pulsed APPJ is observed to produce abundant reactive species and its treatment on deionized water and different cell media leads to PAW and/or PAM which are useful for biomedical applications.

Keywords: nanosecond-pulsed atmospheric pressure plasma jet, plasma activated medium.

1. Introduction

Atmospheric-pressure plasma jets (APPJs) have potential applications in biological decontamination, cancer therapy, and surface treatment. Many of these applications require low-power plasmas with high chemical reactivity at low gas temperature plasmas. Nanosecond-pulsed discharges can generate such nonthermal plasmas [1].

Indirect treatments with plasma activated water (PAW) and /or plasma activated media (PAM) demonstrate similar bactericidal and/or cytotoxic effects as that of direct plasma exposure, but facilitate flexibility and precision of delivery with potentially gentler conditions as may be demanded with *in-vivo* conditions [2, 3].

In our previous studies [3, 4], we have restricted ourselves to the APPJ driven by a low frequency or microsecond-pulsed high voltages. In this work, a high voltage nanosecond-pulsed APPJ is employed for characterizing its plasma properties and utilized to treat the water and different cell media. Characterization of nanosecond-pulsed plasma and its unique features and merits for biomedical applications are explored in comparison with those of low frequency or microsecond-pulsed APPJ.

2. Experimental Setup

The He APPJ consists of an upstream internal stainless steel needle electrode [outer diameter (OD) = 0.9 mm, inner diameter (ID) = 0.6 mm, length = 51 mm] that was sealed with torr-seal into a quartz tube (ID = 1.6 mm and OD = 3 mm), and a downstream external ring copper electrode with length of 4 mm on the outside of the tube. The length of the quartz tube below the needle electrode was fixed to 30 mm [2]. The plasma discharge is produced by applying nanosecond high-voltage pulses between needle electrode and grounded ring copper electrode, as shown in Fig. 1. The application of high-voltage nanosecond-duration pulses generates a strong electric field that accelerates electrons to the high energies required for efficient ionization. Furthermore, the short pulse duration is chosen to prevent spark formation [1]. An FID Technologies generator (Model FPG 20-1NM) is used to produce pulses of width 10 ns (with rise/fall times of 2-3 ns). Helium gas flows in the range of 1 - 6 L/min in the quartz tube.

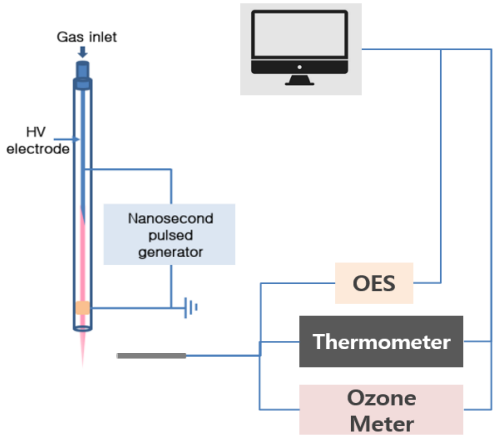

Figure 1. Experimental setup

The optical emission spectrum in range of 200–800 nm recorded from pulsed APPJ is illustrated in Fig. 2. The most intense emission bands were observed between 300 and 400 nm, which correspond to N_2^* second positive system ($C^3\Pi_u \rightarrow B^3\Pi_g$) band head at 337.1 nm and N_2^+ first negative system at 391 nm ($B^2\sum_u^+ \rightarrow X^2\sum_g^+$) [5].

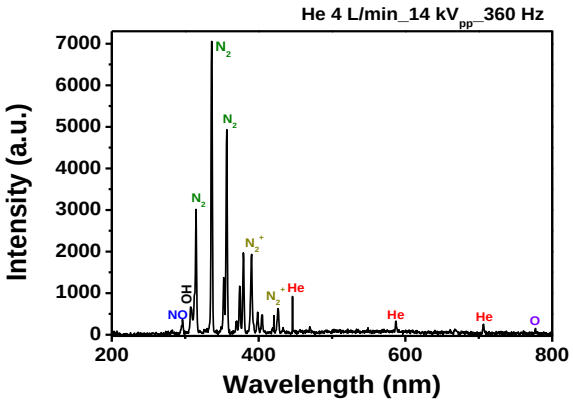

Figure 2. A typical optical emission spectrum of the plasma jet.

The effects of pulse peak voltage and pulse repetition rate on the plasma temperatures (T_{exc}, T_{rot}, and T_{vib}) are evaluated.

During treatment, the gap distance in-between the tube orifice and the surface of the DW/media was kept fixed at 8 mm. The concentrations of the long-lived reactive species such as hydrogen peroxide (H_2O_2), nitrate (NO_3^-), ozone (O_3) in the PAW and PAM were determined spectrophotometrically on the PhotoLab 7600 (WTW, Germany) according to instructions provided by the manufacturer. Nitrite (NO_2^-) concentration was determined using the Griess reagent (Molecular Probes) [5]. The electrical conductivity and the pH of DW were measured with a conductivity meter, OHAUS STARTER ST3100C and a digital pH-meter, OHAUS STARTER ST3100.

3. Discussion

Because the nanosecond high-voltage pulsed discharge is characterized by a fast rise time of pulse voltage, which makes that the electrical energy delivered in discharge is mainly deposited in the energetic electrons instead of heating the heavy particles. Also, the fast rise time of pulse voltage can also improve the energy distribution and make it possible to obtain uniform discharge plasma.

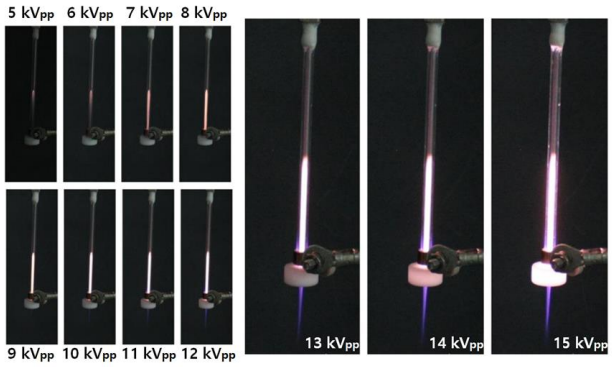

Figure 3. Appearances of the discharge and plume at different applied voltages.

As shown in Fig. 3, at relatively low voltage (around 8 kV_{pp}), plasma generation started as a corona discharge at the tip of the high voltage pin electrode. Raising the applied voltage increased the region of the high electric field, expanding the discharge outward until it transited to a glowing corona at around 10.0 kV_{pp}. Eventually (at around 13.0 kV_{pp}), the charged particles drifted far enough to sense the grounded electrode and the formation of streamers reaching the Petri dish took place. Starting at 14.0 kV_{pp} on, the generation of streamers was stable, and the discharge was distributed throughout the entire funnel volume. Under most of operating condition, the plume temperature remains at room temperature.

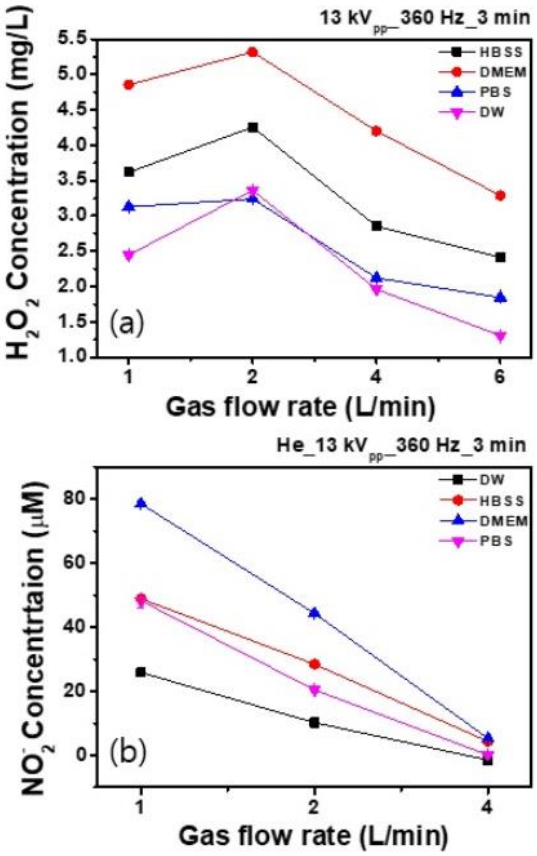

Figure 4. (a) Concentration of H_2O_2 (b)Concentration of NO_2^-.

Figs. 4(a) and 4(b) present the concentrations of H_2O_2 and NO_2^- of the various PAM at several operating conditions. The [H_2O_2] reaches to the highest when the gas flow rate is 2 L/min. The [H_2O_2] in DMEM was higher than those in other media such as HBSS, PBS and DW. On the other hand, the [NO_2^-] decrease with increasing flow rate. Although not shown in the figure, the [H_2O_2] reaches around 15 mg/L at the treatment time of 9 min.

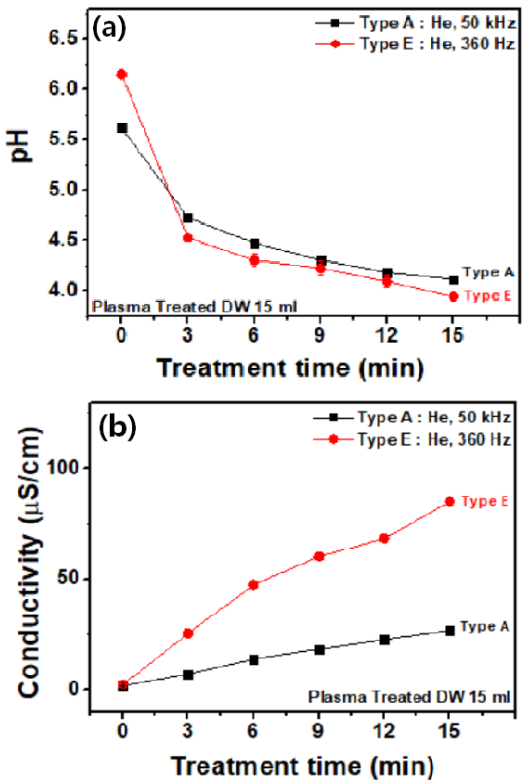

Figure 5. (a) The changes of pH (b) The changes of conductivity for microsecond-pulsed APPJ (type A) and nanosecond-pulsed APPJ (type E).

Figs. 5(a) and 5(b) present the changes of pH and conductivity of the PAW with treatment time. A comparison is made between the microsecond-pulsed APPJ at a moderate voltage and the nanosecond-pulsed APPJ at a high voltage. It should be noted that PAW treated by nanosecond-pulsed high voltage exhibits a drastic drop in pH and a drastic rise in electric conductivity. Oehmigen et al. reported that the main reason for acidification of plasma treated water is the formation of H^+ and HNO_3^- [7]. In Ref. [8], the authors proposed both NO_2^- and NO_3^- to be responsible for the pH drop. However, Vlad et al. suggested that the acidification and electrical conductivity increase in the plasma treated water is due to formation of NO_3^-/HNO_3, the same as in the nitric acid solution [9].

4.Conclusion

In this work, a high voltage nanosecond-pulsed APPJ is fabricated and utilized to treat the deionized water and different cell media. Characterization of nanosecond-pulsed plasma and its unique features and merits for biomedical applications are explored in comparison with those of low frequency or microsecond-pulsed APPJ. Under the normal operating conditions, the APPJ is stably operated and remains at room temperature. Compared to microsecond-pulse APPJ, the nanosecond-pulsed APPJ is observed to produce abundant reactive species due to its high electric field. Its treatment on water and different cell media leads to PAW and/or PAM which are useful for biomedical applications.

5. References

[1] D. Z. Pai et al., Plasma Sources Sci. Technol. **18**, 045030 (2009).

[2] B Ghimire et al., Plasma Sources Sci. Technol. **30**, 035009 (2021).

[3] A. Jo et al., PLoS ONE **17**, e0272805 (2022).

[4] H. M. Joh et al., AIP ADVANCES **7**, 085106 (2017).

[5] Z.-J. Liu et al., Spectrochim. Acta A **121**, 698 (2014)

[6] A. R. Gibson et al., Plasma Process. Polym. **11**, 1142 (2014).

[7] K. Oehmigen et al., Plasma Process. Polym. **7**, 250 (2010).

[8] S. Ikawa, K. Kitano, S. Hamaguchi, Plasma Process. Polym. **7**, 33 (2010).

[9] I.-E. Vlad, S. D. Anghel, Journal of Electrostatics **87**, 284 (2017).